A Detuning-Repeater-Based Dynamic Wireless Charging System With Quasi-Constant Output Power and Reduced Inverter Count

Wenjing Xiong, *Member, IEEE*, Qihui Yu, Zixi Liu, Lei Zhao, *Member, IEEE*, Qi Zhu, and Mei Su, *Member, IEEE*

***Abstract*—High-density coil installation to achieve a smooth power transfer inevitably increases construction costs, reducing the acceptance of dynamic wireless power transfer (DWPT). In this article, a detuning-repeater-based DWPT system is proposed to provide a relatively constant power at a reduced count of inverters. Half of the inverter-connected transmitter coils in conventional DWPT systems are served as passive repeater coils. The repeater relays the power from the transmitters on both sides to take the role of the main power transfer channel when the receiver is moving towards it. A detuning method is proposed to suppress the standby currents inside the idle repeater coils by utilizing the variation of receiver reflecting impedance during the receiver moving towards/away. An optimization method to achieve less power fluctuation is designed based on the detuning rate. The tradeoff between the power fluctuation and current suppression is analyzed. The system performance against parameter variations is also performed. A 100 W down-sized prototype is developed, and the experimental results show that the proposed DWPT system can achieve a quasi-constant output power with a power fluctuation of 8.5% and a system efficiency of around 82% during the entire dynamic process.**

***Index Terms*—Detuning, dynamic wireless power transfer, low construction cost, quasi-constant output power, repeater coil.**

Manuscript received 27 January 2022; revised 26 May 2022; accepted 26 August 2022. Date of publication 5 September 2022; date of current version 10 October 2022. This work was supported in part by the National Natural Science Foundation of China under Grant 61933011 and Grant 62125308, in part by the Hunan Provincial Natural Science Foundation of China under Grant 2020JJ5753, and in part by the Project of Innovation-Driven Plan in Central South University. Recommended for publication by Associate Editor C. Fernandez. *(Corresponding author: Zixi Liu.)*

Wenjing Xiong, Qihui Yu, Zixi Liu, and Mei Su are with the School of Automation, Central South University, Changsha 410083, China, and also with the Hunan Provincial Key Laboratory of Power Electronics Equipment and Grid, Central South University, Changsha 410083, China (e-mail: csu.xiong@163.com; csu_yuqihui@163.com; zgliuzixi@163.com; sumeicsu@csu.edu.cn).

Lei Zhao is with the College of Automation, Chongqing University, Chongqing 400044, China (e-mail: lzha915@aucklanduni.ac.nz).

Qi Zhu is with the Beijing Xiaomi Mobile Software Co., Ltd., Beijing 100085, China (e-mail: zhuqi3@xiaomi.com).

Color versions of one or more figures in this article are available at https://doi.org/10.1109/TPEL.2022.3204054.

Digital Object Identifier 10.1109/TPEL.2022.3204054

NOMENCLATURE

V_{in}	Dc-side voltage.
V	Rms value of the fundamental wave of the inverter output voltage.
V_{inv}	Output square-wave voltage of the inverter.
$V_{\text{ON\_}re}$	Induced voltage on the receiver coil.
V_{re}	Load voltage.
ω	Operating angular frequency.
f	Operating frequency.
M_{ar1}	Mutual inductance between active coil 1 and receiver coil.
M_{ar2}	Mutual inductance between active coil 2 and receiver coil.
M_{ap}	Mutual inductance between active coil and repeater coil.
M_{pr}	Mutual inductance between repeater coil and receiver coil.
L_{ac1} & L_{ac2}	Self-inductance of active coil 1, 2.
L_{rp}	Self-inductance of repeater coil.
L_{re}	Self-inductance of receiver coil.
L_{T1} & L_{T2}	Resonant inductance of active coil 1, 2.
r	Parasitic resistance of L_{ac1}, L_{ac2}, L_{rp}, L_{T1}, L_{T2}.
r_e	Parasitic resistance of L_{re}.
C_{ac1} & C_{ac2}	Resonant capacitor of active coil 1, 2.
C_{rp}	Resonant capacitor of repeater coil.
C_{re}	Resonant capacitor of receiver coil.
R	Load.
Z_{rp}	Input impedance of repeater coil.
I_{p1} &I_{p2}	Inverter output current of active coil 1, 2.
I_{ac1} &I_{ac2}	Current of active coil 1, 2.
I_{rp}	Current of repeater coil.
I_{re}	Current of receiver coil.
θ	Phase angle between $V_{\text{ON\_}re}$ and I_{re}.
P_{out}	Output power.
$P_{\text{out,AR}}$	Output power in AR charging mode.
$P_{\text{out,PR}}$	Output power in PR charging mode.
P^*_{out}	Rated output power.
$P_{\text{out-max}}$	Maximum output power.
$P_{\text{out-min}}$	Minimum output power.
α	Detuning rate of repeater coil.
β	Detuning rate of receiver coil.
η	System efficiency.

D	Distance between the center of the road coils.
h	Hight of air gap.

I. Introduction

THE technology of wireless power transfer (WPT) is getting popularity in many practical applications, due to its advantages of convenience, high safety, and low maintenance cost compared to traditional plug-in charging [1], [2]. According to the movement status of the receiver, wireless charging systems can be categorized into static wireless power transfer (SWPT) systems and dynamic wireless power transfer (DWPT) systems. The SWPT system, with a stationary receiver, has been widely applied in mobile devices [3], biomedical implantation [4], electric vehicles (EVs) [5], and automated guided vehicles (AGVs) [6]. In the field of SWPT, researchers mainly focus on improving transmitting distance, optimizing system efficiency, and improving misalignment tolerance through the design of magnetic coupling structure, compensation network, and control method [7], [8], [9]. However, large capacity battery and long charging time are still to be issues in SWPT systems [10], [11], [12].

DWPT has received more attention over the worldwide wireless power researchers, which is filling the gaps for the aforementioned defects in SWPT. The dependence on the battery capacity of the receiver can be greatly reduced in DWPT systems owing to its ability to charge the moving receiver [10], [11]. Because of this characteristic, DWPT becomes an ideal charging method for AGVs and EVs. In the literature, there are two common types of coil tracks for DWPT systems: stretched and lumped. The stretched track contains one road coil with a much larger dimension than the receiver coil. The lumped track contains a string of road coils that has a similar size to the receiver coil [12]. Unlike the stretched track, the lumped track only activates the track coil coupled with the receiver. Thereby, the lumped one has lower power losses and can avoid the radiation from the uncoupled track portions. According to the current research status, three main challenges limit the development of the DWPT system with lumped track [13], [14]. 1) low efficiency during the dynamic process; 2) low tolerance of receiver misalignment; and 3) high construction cost.

Many studies have been developed to address the above challenges. Segmentation control proposed in [15], [16], [17], and [18] can improve the system efficiency by keeping the uncoupled coils of the system turned OFF. However, the power transfer fluctuates greatly as the alignment status of the receiver and transmitter varies. To maintain the power transfer under receiver misalignment conditions, a DDQ pads structure is proposed and the charging zone is expanded 5 times larger than the ordinary circular coils [19]. As well, a hybrid WPT system combined *LC* and *LCL* resonant compensation owns an excellent tolerance for pad misalignment with only $\pm 5\%$ power fluctuation [20]. Moreover, an optimized current control method by adjusting the currents of transmitters can achieve constant output power with high efficiency in an overlapped coil structure [21]. But these systems need extra ferrite bars, coils, or complicated controllers, which increases the construction cost. In [22] and [23], the scheme has a central power supply feeding a power rail with the advantages of fewer electronics components and installation cost. But the loss in the power cable connecting the segments is high. In the abovementioned researches, there are still some practical difficulties during implementation.

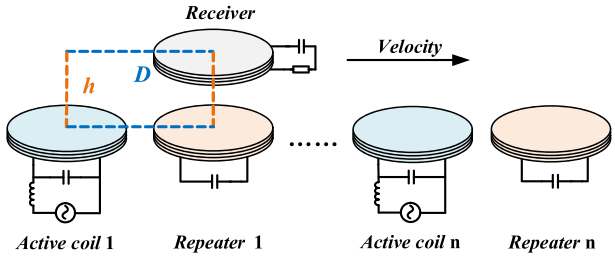

Fig. 1. Proposed DWPT system.

To achieve smooth power transfer under a low-cost structure, this article proposes a detuning-repeater-based DWPT system where half of the converter-driven transmitters are replaced by passive repeater coils. That is lower the installation cost as the number of inverters and resonant elements has been reduced. The receiver and repeater coils are designed under detuning through resonant capacitor selection. Based on that, the uncoupled repeater coil can be automatically restrained to a low power state that reduces the no-load loss and benefits the system safety. Additionally, as the receiver coil moves towards the repeater coil, the current of the repeater coil will increase gradually. The detuning effect will be eliminated by the reflective impedance of the receiver, and the repeater coil will become the main channel of power transfer gradually. The current variation of the repeater coil is dependent on the detuning degrees, which can be characterized by the detuning rates while the power fluctuation can be minimized by the selection of the detuning rate.

In the rest of this article, the proposed DWPT system is modeled, and the equivalent circuit model of the basic DWPT unit under different operation conditions is analyzed in Section II. In Section III, different detuning types are studied and compared. The boundary condition of the current suppression and power fluctuation is studied and the system performance against parameter variations is analyzed. The detuning-rate-based design procedure is given. In Section IV, a 100 W experimental prototype is built to verify the feasibility of the proposed DWPT system. Finally, Section V concludes this article.

II. System Modeling and Analysis

A. Overall Structure of Repeater-Based DWPT System

The overall structure of the repeater-based DWPT system is shown in Fig. 1, where the road coils are alternately arranged by active coils and repeater coils. The active coils are *LCL* compensated, while the repeater coils are series compensated as well as the receiver coil. Compared to the traditional DWPT system, the proposed system saves half the amount of the inverters. The specifications of the road coils are all the same. When the receiver coil moves along the road, the active coils and the repeater coils alternately become the main channel of power transfer.

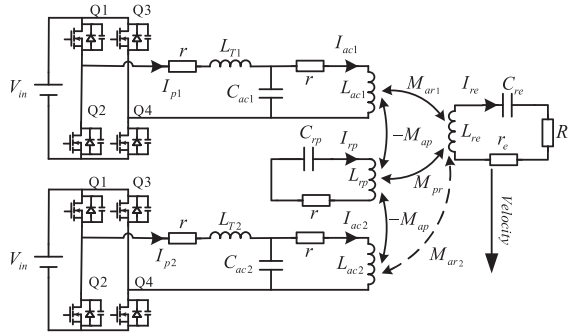

Fig. 2. Schematic of the proposed DWPT system.

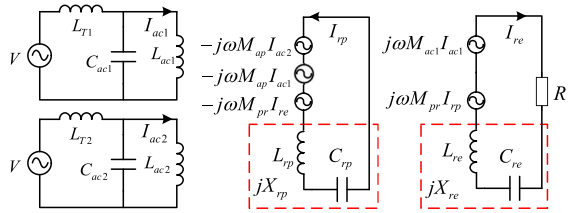

Fig. 3. Simplified circuit of the proposed DWPT system.

B. Modeling of the Repeater-Based DWPT System

To clarify the operation principle of the proposed DWPT system, the schematic of the proposed DWPT unit shown in Fig. 2 is analyzed as an example. The relationship between the self-inductance is that $L_{Ti} = L_{aci} = L_{rp} = L(i = 12)$. Compared to M_{ar1} and M_{pr}, M_{ar2} is small enough to be ignored. The minus sign in front of M_{ap} indicates that the direction of the magnetic flux passing through the repeater coils is opposite to that of the receiver coil. For simplification, the parasitic resistances of these elements are neglected. The resonant condition of the active coil can be derived as

$$\omega = 2\pi f = \frac{1}{\sqrt{L_{Ti}C_{aci}}} = \frac{1}{\sqrt{L_{aci}C_{aci}}}(i = 1, 2). \tag{1}$$

The dc voltage supply, full-bridge inverter, and *LCL* compensation network of the active coil can be simplified as a constant current source [24]. The current can be calculated as

$$I_{aci} = \frac{V}{j\omega L}(i = 1, 2) \tag{2}$$

where $V = \frac{2\sqrt{2}}{\pi}\ V_{\text{in}}$.

The simplified circuit model of the proposed DWPT system is shown in Fig. 3. The repeater and receiver coil are designed to be detuned, which means that the coil and resonant capacitors are not in fully-tuned condition [25]. The imaginary impedance of the repeater coil loop and receiver coil loop can be expressed as

$$\begin{cases} X_{rp} = \omega L_{rp} - \frac{1}{\omega C_{rp}} \\ X_{re} = \omega L_{re} - \frac{1}{\omega C_{re}}. \end{cases} \tag{3}$$

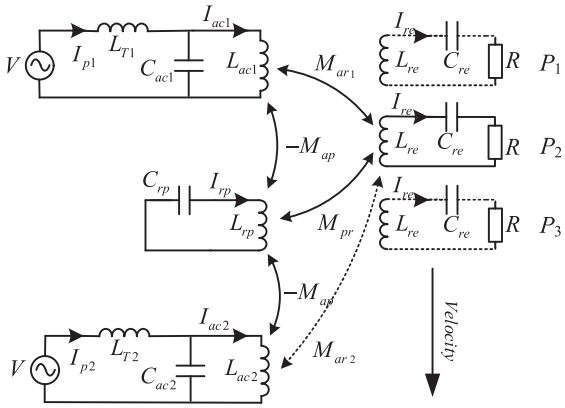

Fig. 4. Different charging modes of the proposed system.

According to the KVL's law, the detailed circuit model of the proposed system is shown as follows:

$$\begin{bmatrix} j\omega M_{pr} & -jX_{rp} \\ -(R + jX_{re}) & j\omega M_{pr} \end{bmatrix} \begin{bmatrix} I_{re} \\ I_{rp} \end{bmatrix} + \begin{bmatrix} 2j\omega M_{ap} \\ j\omega M_{ar1} \end{bmatrix} I_{ac1} = \begin{bmatrix} 0 \\ 0 \end{bmatrix}. \tag{4}$$

The detuning rate is introduced to characterize the intensity of the detuning effect of the coils, which is expressed as

$$\begin{cases} \alpha = \frac{X_{rp}}{\omega L_{rp}} \\ \beta = \frac{X_{re}}{\omega L_{re}}. \end{cases} \tag{5}$$

Submitting (2), (3), (5) into (4), the currents in the repeater coil and the receiver coil can be derived as

$$\begin{cases} I_{re} = \frac{V(\alpha L M_{ar1} + 2M_{ap}M_{pr})}{L(\alpha LR + j(\alpha\beta\omega LL_{re} - \omega M_{pr}^2))} \\ I_{rp} = \frac{V(\omega M_{ar1}M_{pr} + 2\beta\omega L_{re}M_{ap} - 2jRM_{ap})}{L\omega(\alpha LR + j(\alpha\beta\omega LL_{re} - \omega M_{pr}^2))}. \end{cases} \tag{6}$$

From Fig. 3, the induced voltage on the receiver coil is shown in

$$V_{on\_re} = j\omega M_{ar1}I_{ac1} + j\omega M_{pr}I_{rp}. \tag{7}$$

The load power can be expressed as

$$P_{\text{out}} = |V_{\text{on\_re}}|\,|I_{re}|\cos(\theta). \tag{8}$$

The losses of the system mainly lie in the parasitic resistances of the coils. Hence, the expression of system efficiency can be simplified as

$$\eta = \frac{P_{\text{out}}}{P_{\text{out}} + 2I_{ac1}^2 r + I_{rp}^2 r + I_{p1}^2 r + I_{p2}^2 r + I_{re}^2 r_e}. \tag{9}$$

C. Circuit Analysis of Different Operation Modes

Depending on the position of the receiving coil, the dynamic process can be divided into three different charging modes as shown in Fig. 4.

1) Active-Receiver (AR) Charging Mode: When the receiver coil is aligned with the active coil at the position of P_1, the system operates in AR charging mode. The equivalent circuit is shown in Fig. 4. As the receiver coil is far from the repeater coil, the mutual inductance M_{pr} and M_{ar2} can be ignored. Thus, (6)

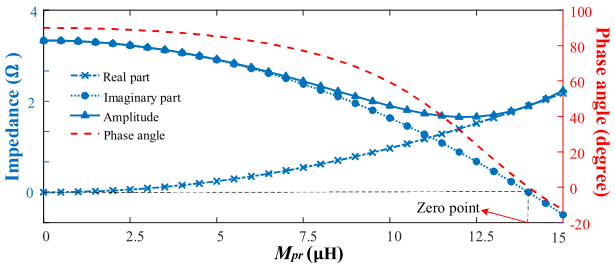

Fig. 5. Variations of the real part, imaginary part, amplitude, and phase angle of Z_{rp} against M_{pr}.

can be rewritten as

$$\begin{cases} I_{re} = \frac{VM_{ar1}}{LR+j\beta\omega LL_{re}} \\ I_{rp} = -\frac{2jVM_{ap}}{\alpha\omega L^2}. \end{cases} \tag{10}$$

In AR charging mode, the power is mainly transferred through the active coil, and the repeater coil is almost uncoupled with the receiver coil. If the repeater coil is fully compensated by its series-connected capacitor, the repeater circuit would turn into a short circuit condition. As indicated in (10), there will be an extremely high current in the repeater coil when $\alpha = 0$, which leads to high no-load loss and a dramatic decrease in system efficiency. To avoid the system being destroyed by the high no-load current in the repeater coil, an imaginary impedance is introduced here by artificially setting the value of α not equal to zero. In this way, the repeater coil turns into a detuning condition. In this condition, the repeater current can be restrained to a low level, while the power transfer from the active coil to the receiver would not be affected. So that the system safety can be guaranteed and the system efficiency improves.

2) Repeater-Receiver (PR) Charging Mode: When the receiver coil is right above the repeater coil at the position of P_3 shown in Fig. 4, the system operates in PR charging mode. Different from AR charging mode, the receiver coil is strongly coupled with the repeater coil, and the power is mainly transferred by the repeater coil. The mutual inductance M_{ar1} and M_{ar2} can be ignored. In this mode, (6) can be rewritten as

$$\begin{cases} I_{re} = \frac{2VM_{ap}M_{pr}}{L(\alpha LR+j(\alpha\beta\omega LL_{re}-\omega M_{pr}^2))} \\ I_{rp} = \frac{2V\beta\omega L_{re}M_{ap}-2jVRM_{ap}}{L\omega(\alpha LR+j(\alpha\beta\omega LL_{re}-\omega M_{pr}^2))}. \end{cases} \tag{11}$$

To enhance the power transfer ability of the repeater channel, the detuning effect on the repeater coil needs to be attenuated in PR charging mode. In this mode, as M_{pr} gets much stronger than that in AR mode, the reflected impedance from the receiver can be used to eliminate the imaginary impedance of the repeater circuit. The detuning effect of the repeater coil can be completely faded away by designing β. The reflexive impedance of the receiver and input impedance of the repeater circuit can be derived as

$$Z_{rp} = \frac{R\omega^2 M_{pr}^2}{A} + j\alpha\omega L_{rp} - \frac{j\beta\omega^3 M_{pr}^2 L_{re}}{A} \tag{12}$$

where $A = R^2 + (\beta\omega L_{re})^2$.

Fig. 5 shows that the real part of Z_{rp} is positively correlated with M_{pr} while the imaginary part is reversed. With the increase of M_{pr}, the imaginary part of Z_{rp} decreases and there is a zero-crossing point. Calculated by $\mathrm{Im}[Z_{rp}] = 0$, the following equation can be obtained:

$$\frac{\beta\omega^2 L_{re}M_{pr}^2}{\alpha L\left(R^2+\beta^2\omega^2 L_{re}^2\right)} = 1. \tag{13}$$

Substitute (13) into (11), the current expression can be rewritten as

$$\begin{cases} I_{re} = \frac{2VM_{ap}(jR+\beta\omega L_{re})}{LR\omega M_{pr}} \\ I_{rp} = \frac{2VM_{ap}(R^2+\beta^2\omega^2 L_{re}^2)}{LR\omega^2 M_{pr}^2}. \end{cases} \tag{14}$$

From (14), if the imaginary impedance of the repeater loop is zero, V and I_{rp} are in the same phase with a 90° leading to I_{ac1}. From the entire dynamic process, the output power fluctuation of AR and PR charging modes are not supposed to be large. Once the induced voltages on the receiver coil in AR and PR charging modes are in the same amplitude, the output power in AR and PR charging modes will be the same. The constraint of the output power in AR and PR charging modes can be mathematically described as

$$|j\omega M_{ar1}I_{ac1}| = |j\omega M_{pr}I_{rp}|. \tag{15}$$

Combining (2), (14), and (15), this condition can be simplified as

$$X_{re} = \sqrt{\frac{\omega M_{pr}M_{ar1}R}{2M_{ap}} - R^2}. \tag{16}$$

3) Active-Repeater-Receiver (APR) Charging Mode: When the receiver coil is between the active coil and repeater coil at the position of P_2 shown in Fig. 4, the system operates in APR charging mode. In APR charging mode, the active coil and repeater coil are coupled with the receiver coil and supply power to the receiver simultaneously. The currents of the repeater and receiver coil can be calculated by (6). This is a transition charging mode in which the main power transfer channel is converted from the active coil to the repeater coil. The output power fluctuation will reach its maximum in APR charging mode for the dynamic variation of M_{ar1} and M_{pr}. As mentioned before, the detuning effect of the repeater coil can be eliminated with the receiver moving towards the repeater. I_{rp} will increase and the induced voltage generated by the repeater coil will increase as well, which can compensate for the decrease in that of the active coil and maintain the smoothness of $V_{\mathrm{on\_}re}$ according to (7). In consequence, the smoothness of the output power can be guaranteed. λ is defined as a parameter characterizing the fluctuation of output power, as shown in

$$\lambda = \begin{cases} \frac{P_{\mathrm{out\_max}}-P_{\mathrm{out}}^*}{P_{\mathrm{out}}^*}, \text{when}: P_{\mathrm{out\_max}} - P_{\mathrm{out}}^* \geq |P_{\mathrm{out\_min}} - P_{\mathrm{out}}^*| \\ \frac{P_{\mathrm{out\_min}}-P_{\mathrm{out}}^*}{P_{\mathrm{out}}^*}, \text{when}: P_{\mathrm{out\_max}} - P_{\mathrm{out}}^* < |P_{\mathrm{out\_min}} - P_{\mathrm{out}}^*|. \end{cases} \tag{17}$$

III. Detuning Method and System Parameter Analysis

A. Detuning Type Analysis

In general, the repeater coil can be designed as inductive or capacitive detuning. According to (3) and (5), when α>0, the

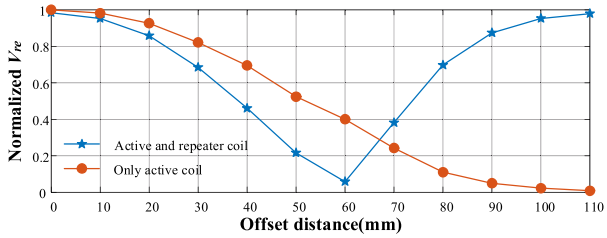

Fig. 6. Normalized V_{re} variation against the offset distances (capacitive detuning).

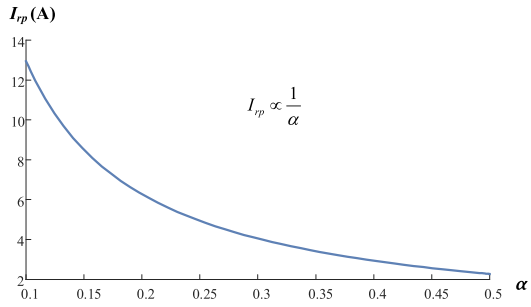

Fig. 7. I_{rp} variation against α (inductive detuning).

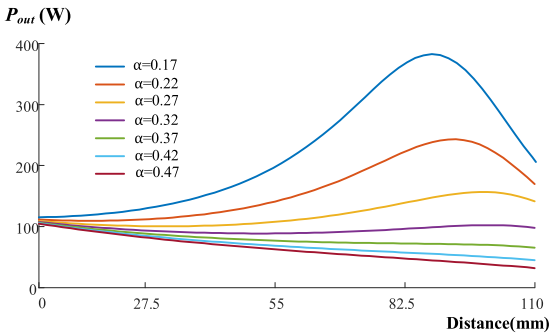

Fig. 8. P_{out} variation against α.

repeater circuit is inductive detuning, when $\alpha<0$, it is capacitive detuning. The current of the repeater coil can be calculated as

$$I_{rp} = \frac{2j\omega M_{ap} I_{ac1}}{Z_{rp}}. \tag{18}$$

When the system operates in AR charging mode, it can be rewritten as

$$I_{rp} = \frac{2M_{ap} I_{ac1}}{\alpha L_{rp}}. \tag{19}$$

From (19), if the repeater coil is capacitive detuning where $\alpha<0$, the phase between the repeater current I_{rp} and active coil current I_{ac1} is π. The induced voltages they generate on the receiver coil will cancel each other out based on (7). When the receiver moves, the values of M_{ar1} and M_{pr} change in the opposite direction. Consequently, there must be a specific position where the induced voltage reaches zero. On the contrary, if the repeater coil is inductive detuning ($\alpha>0$), the current directions of the repeater and active coil will be the same. In this state, the induced voltages will add each other to maintain the quasi-constant power transfer during the dynamic process.

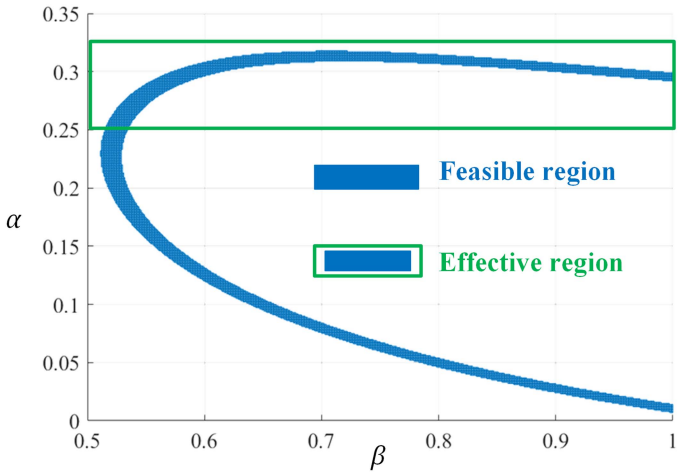

Fig. 9. Effective region of α, β within the power fluctuation.

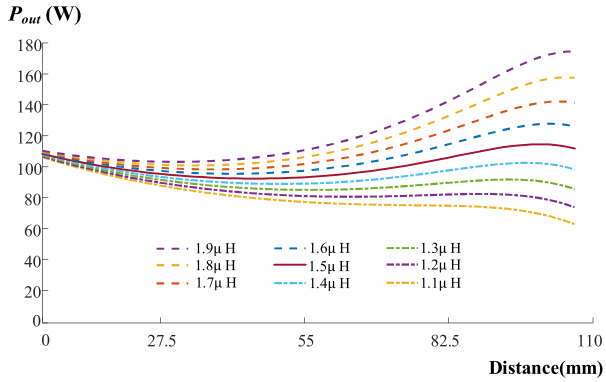

Fig. 10. P_{out} under different M_{ap}.

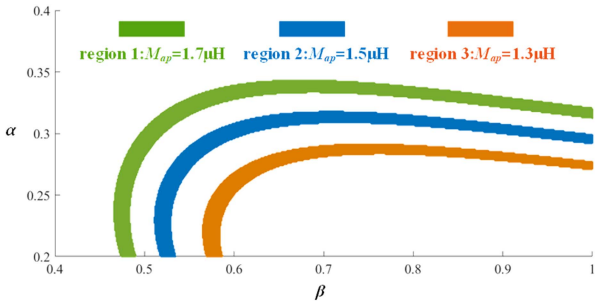

Fig. 11. Effective region under various M_{ap}.

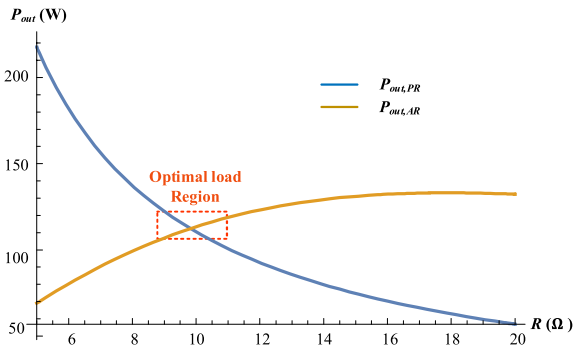

Fig. 12. $P_{\text{out,AR}}$ and $P_{\text{out,PR}}$ variation against load.

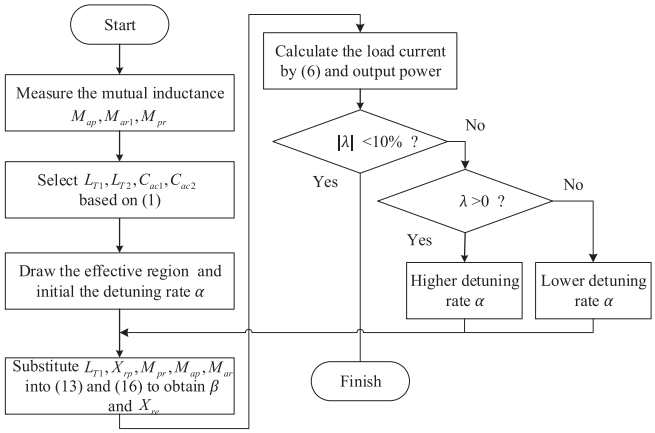

Fig. 13. Flow chart of the design procedures of the proposed DWPT system.

Furthermore, the detuning types of the repeater and receiver coils must be the same. The impedance reflecting will reverse the type of imaginary impedance of the receiver. If the type of imaginary impedance of the receiver is inconsistent with that of the repeater, the reflected impedance of the receiver will be consistent with that of the repeater. It will enlarge the imaginary impedance in the repeater circuit, rather than eliminate the detuning impedance based on (12). As a result, the power transfer from the repeater to the receiver will be blocked more severely.

The simulation result of the capacitive detuning in both repeater and receiver coils is shown in Fig. 6 by using MATLAB/Simulink. The offset distance is the misalignment distance between the receiver coil and the active coil 1. When the offset distance equals zero, the receiver is aligned with the active coil 1 while the offset distance equals 110 mm, which means the receiver is right above the repeater coil, as shown in Fig. 1. The blue line presents the load voltage activated by the active coil and repeater coil simultaneously while the red line presents that activated by the active coil only. As illustrated in Fig. 6, with the offset distance increasing, the blue line decreases first, after reaching the minimum value at 60 mm, and then increases. While the red line monotonically decreases with the increment of the offset distance. Besides, the red line keeps higher than the blue line before the offset distance reaches 60 mm. It is because the load voltage generated by the active coil is eliminated by that of the repeater coil. With the movement of the receiver, the load voltage generated by the active coil decreases and is larger than that of the repeater coil before the offset distance reaches 60 mm. On the contrary, the load voltage generated by the repeater coil increases and is larger than that of the active coil after the offset distance reaches 60 mm. As a result, the capacitive detuning will lead to a large power fluctuation in APR charging mode and is not applicable here. The following analysis of the proposed system is under the inductive detuning situation.

B. Detuning Rate Analysis

It can be known that the currents of the repeater and receiver coil are drastically affected by the detuning rate, and a larger α (α>0) will result in a smaller repeater current, as shown in Fig. 7. However, in APR charging mode, the repeater circuit needs

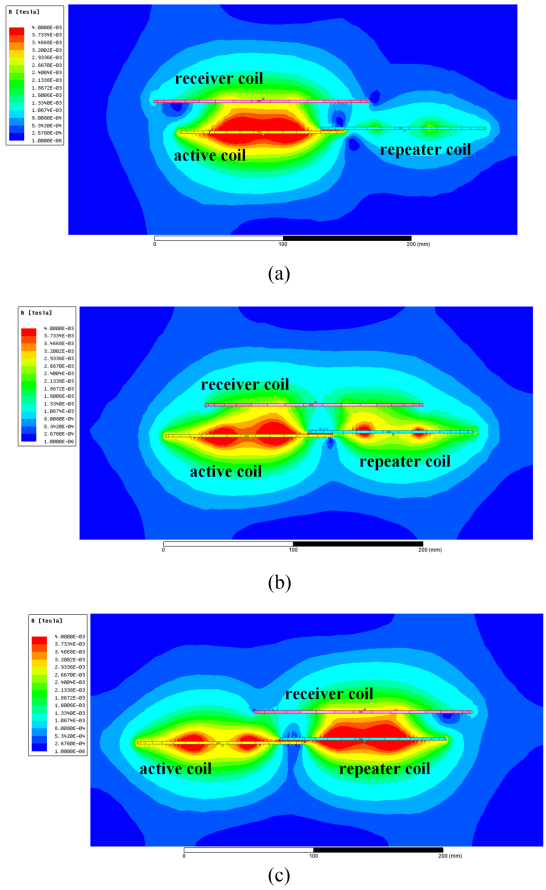

Fig. 14. Magnetic field distribution (inductive detuning). (a) AR charging mode. (b) APR charging mode. (c) PR charging mode.

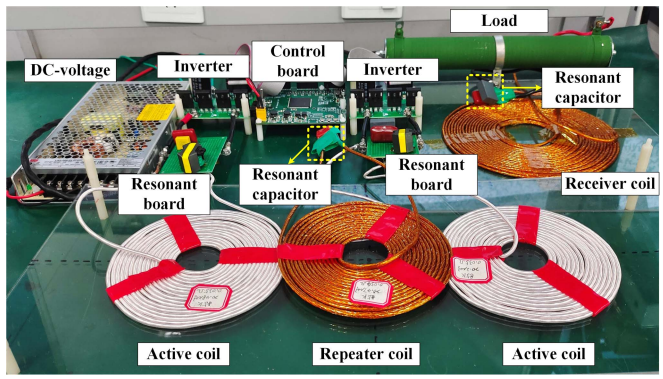

Fig. 15. 100 W experimental setup.

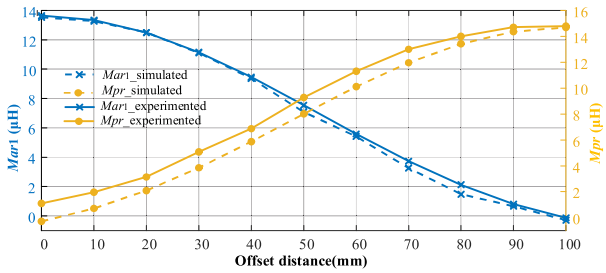

Fig. 16. M_{ar1} and M_{pr} variation against the offset distances.

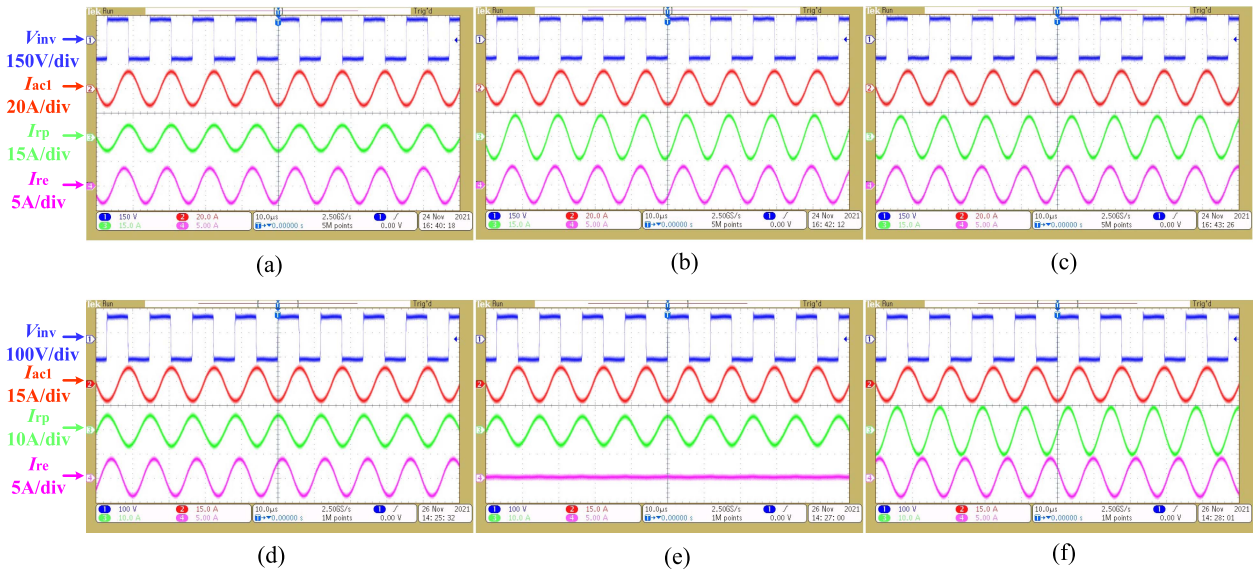

Fig. 17. Waveforms of V_{inv}, I_{ac1}, I_{rp}, I_{re} in different charging modes: Inductive detuning (a) AR charging mode. (b) APR charging mode. (c) PR charging mode. Capacitive detuning. (e) AR charging mode. (d) APR charging mode. (f) PR charging mode.

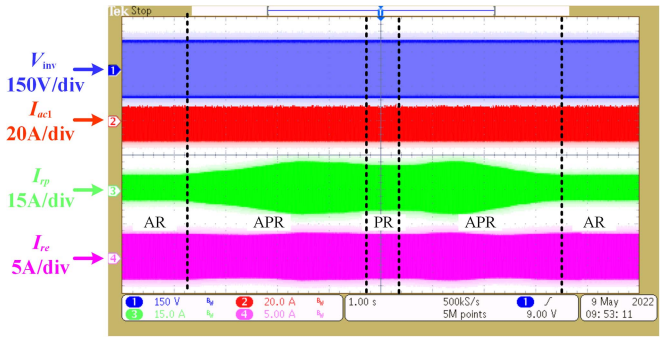

Fig. 18. Waveforms in the whole dynamic process.

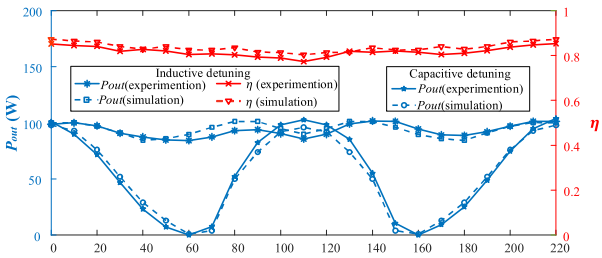

Fig. 19. Output power and system efficiency variations against the offset distances.

a larger current to enhance the power transfer. Because when M_{ar1} decreases, the repeater coil is gradually taking the key role of power transfer. If the imaginary impedance in the repeater circuit is too large to be eliminated, I_{rp} will be suppressed by the detuning effect all the time, which results in lower output power. On the contrary, if the imaginary impedance is too small, the excessive increase of I_{rp} will result in a severe output power fluctuation. In consequence, the detuning rate should be properly selected for the mitigation of power fluctuation and maintaining a quasi-constant output power.

TABLE I
SIMULATION PARAMETERS OF THE PROPOSED DWPT SYSTEM

Parameter	Value	ESR
L_{T1}& L_{T2}& L_{ac1}& L_{ac2}	20 μH	0.035 Ω
C_{ac1}& C_{ac2}	175 nF	0.030 Ω
L_{re}	54.5 μH	0.060 Ω
C_{re}	133 nF	0.030 Ω
C_{rp}	252 nF	0.030 Ω
M_{ap}	1.46μH	
R	10Ω	
V_{in}	120V	

The system parameters used in this section are shown in Table I. The effects of different α on P_{out} in the dynamic process are shown in Fig. 8. It can be seen that a larger α gets a lower average output power while a smaller α gets a higher average output power. Neither α is too high nor too low, there will be an unexpected power fluctuation in the dynamic process, which is consistent with the abovementioned analysis. During the whole dynamic process, the output power can be derived as

$$P_{\text{out}} = \frac{RV^2(\alpha L M_{ar1} + 2M_{ap}M_{pr})^2}{L^2\left(\alpha^2R^2L^2 + (\alpha\beta\omega L L_{re} - \omega M_{pr}^2)^2\right)}. \tag{20}$$

Let $M_{ar1} = 0$ or $M_{pr} = 0$ in (20), the output power under AR and PR charging mode can be obtained

$$\begin{cases} P_{\text{out,AR}} = \dfrac{RV^2M_{ar1}^2}{L^2(R^2+\beta^2\omega^2L_{re}^2)} \\ P_{\text{out,PR}} = \dfrac{4RV^2M_{ap}^2M_{pr}^2}{L^2\left(\alpha^2R^2L^2+(\alpha\beta\omega L L_{re}-\omega M_{pr}^2)^2\right)}. \end{cases} \tag{21}$$

From Fig. 8, it can be found that the closer the output power in AR and PR modes are, the smaller the power fluctuation will be. A factor δ is defined to represent the relative power fluctuation,

which is shown as follows:

$$\delta = \frac{P_{\text{out,AR}}}{P_{\text{out,PR}}}. \tag{22}$$

On this basis, the acceptable region of detuning rates α and β is shown in Fig. 9. The feasible region is selected as $\delta \in [0.95,\ 1.05]$, where the power fluctuation is relatively low. In order to characterize the suppression degree of the no-load repeater current, ξ is defined by I_{rp}/I_{ac1} in AR charging mode

$$\xi = \left| \frac{2\omega M_{ap}}{r + \alpha L} \right|. \tag{23}$$

To effectively suppress the no-load current, the condition where $\xi < 0.5$ should be satisfied in the proposed system. Referring to the system parameters in Table I, α should be larger than 0.25. Therefore, the effective region is only the upper part of the feasible region. The upper boundary of α is 0.31 where the no-load current is minimized. If α is larger than 0.31, δ is out of the feasible region no matter what the value β is. The reason why β is set within 0 and 1 is that higher detuning impedance on the receiver side will result in a low voltage gain and low efficiency.

C. Analysis of System Parameters Variations

1) Variation of M_{ap}: According to (18) and (19), I_{rp} is proportional to M_{ap} as the induced voltage on the repeater coil is increased when the coupling between the active and the repeater coils gets higher. The effect of M_{ap} on the output power is shown in Fig. 10. As illustrated, the output power is hardly influenced by the variation of M_{ap} in AR charging mode, while it increases with M_{ap} in APR and PR charging modes due to a higher I_{rp}.

The effective region of detuning rates under various M_{ap} is shown in Fig. 11. To ensure ξ<0.5 under all the values of M_{ap}, the constraint of α is set as α>0.2. With the same β, a larger M_{ap} needs a higher detuning rate α to maintain a smooth power transfer by suppressing I_{rp}. On the other side, with the same α, a larger M_{ap} needs a smaller β, which can be derived from (14). In order to satisfy the constraint of the output power in (15), I_{rp} needs to maintain constant against parameter variations in PR charging mode. Thus, if M_{ap} increases, β is supposed to be decreased. In conclusion, the power fluctuation caused by the strengthening of M_{ap} can be reduced by the increase of α or the decrease of β.

2) Load Variation: In practical application, the equivalent load always varies with different charging requirements. Thus, the performance of the proposed system should be evaluated in terms of load variation. The variations of $P_{\text{out,AR}}$, and $P_{\text{out,PR}}$ against load variation are shown in Fig. 12. It can be seen that $P_{\text{out,AR}}$, is positively while $P_{\text{out,PR}}$ is negatively correlated with the load in a certain range. The optimal load region is around 10 Ω when the system parameters are selected, as shown in Table I. To further analyze the parameters that affect the optimal load region, (20) can be rewritten as

$$P_{\text{out}} = \frac{\text{V}^2 (L\alpha M_{ar1} + 2M_{ap}M_{pr})^2}{L^2} + \frac{1}{\text{AR} + \frac{B}{R}} \tag{24}$$

where $A = L^2\alpha^2, B = (L\alpha\beta\omega L_{re} - \omega M_{pr}^2)^2$. Referring to (24), when the relative position of the coils is fixed, the optimal load region is only determined by the detuning rates α and β.

D. Parameter Design Consideration

In order to illustrate how to design the detuning-repeater-based DWPT system, the flow chart of the design procedures is shown in Fig. 13. The frequency is selected as 85 kHz according to SAE international standard. The detailed design procedures are listed as follows.

1) Measure the mutual inductances M_{ar1}, M_{ap}, M_{pr} by the formula $V = j\omega MI$.
2) Select the resonant element parameters C_{ac1}, C_{ac2}, L_{T1}, L_{T2} of the active coil by (1).
3) Draw the effective region as Fig. 9 according to the measured parameters, and initial the detuning rate α.
4) Substitute $L_{T1}, X_{rp}, M_{ar1}, M_{ap}, M_{pr}$ into (13) and (16) to obtain β and X_{re}.
5) Calculate the load current by (6) during the entire dynamic process. Then, calculate P_{out}, λ.
6) Determine whether |λ|<10%. If yes, the design is finished. If not, go to step (7).
7) Determine whether λ>0. If yes, select a larger C_{rp} and obtain a higher detuning rate α. If not, select a smaller C_{rp} and obtain a lower detuning rate α. Then, go to step (5).

IV. Simulation and Experimental Results

A. Simulation Results

The magnetic field distribution in different charging modes is shown in Fig. 14 by using the FEM tool Maxwell three-dimensional.

There is a slight overlap between the active and the repeater coil to increase the coupling between them. In Fig. 14(a), the magnetic field around the active coil is much more intensive than that of the repeater coil. This is because the active coil is the power transfer channel and the repeater coil is suppressed at a low power consumption state by the detuning effect. In Fig. 14(b), the magnetic field intensity of the active coil is weaker while that of the repeater coil is stronger compared to AR charging mode. The power transferred by the active coil is reduced due to the weak coupling with the receiver. Meanwhile, the repeater current has increased and started to transfer power to the receiver coil. In Fig. 14(c), the magnetic field intensity of the active coil is the weakest while that of the repeater coil is the strongest in all charging modes. The repeater coil current further increases and has become the main channel for power transfer. Meanwhile, the active coil is excited by a voltage source and still has a certain magnetic field strength. In summary, with the receiving coil approaching, the repeater coil can be gradually activated from a low power consumption state to a power transfer state.

B. Experimental Setup

To verify the feasibility of the proposed detuning-repeater-based DWPT system, a 100 W experimental prototype was built

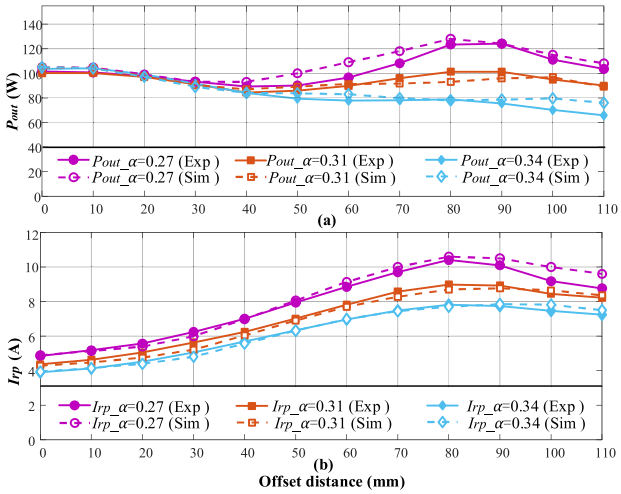

Fig. 20. (a) P_{out} under various detuning rates. (b) I_{rp} under various detuning rates.

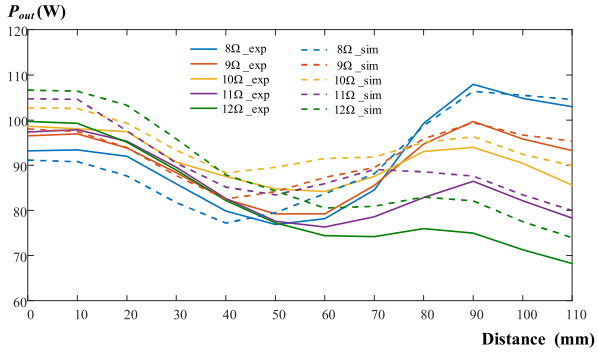

Fig. 21. P_{out} variation against R.

TABLE II
PARAMETERS OF THE PROPOSED DWPT SYSTEM

Parameter	Value	ESR
L_{T1}	20.07 μH	0.032 Ω
L_{T2}	20.40 μH	0.031 Ω
C_{ac1}	174.70 nF	0.028 Ω
C_{ac2}	171.77 nF	0.026 Ω
L_{ac1}	20.20 μH	0.035 Ω
L_{ac2}	20.48 μH	0.035 Ω
L_{rp}	20.2 μH	0.035 Ω
L_{re}	54.49 μH	0.060 Ω
C_{re}(Inductive detuning)	132.70 nF	0.026 Ω
C_{re}(Capacitive detuning)	36.20 nF	0.033 Ω
C_{rp}(Inductive detuning)	252 nF	0.027 Ω
C_{rp}(Capacitive detuning)	133.35 nF	0.029 Ω
M_{ap}	1.46 μH	
R	10.4 Ω	
Vin	120 V	

TABLE III
POWER FLUCTUATION UNDER DIFFERENT R

Load Variation	Power Fluctuation (Sim)	Power Fluctuation (Exp)
-20%	13.5%	15.5%
-10%	9%	9.5%
0	7%	8.5%
10%	12%	11.6%
20%	17%	17.5%

in the lab with OFF-the-shelf components, as shown in Fig. 15. The air gap h is 25 mm and the distance between the center of the road coils D is 110 mm. The PWM signals driving the inverter with a phase shift angle of 90° are generated by a DSP controller of TMS320F28335. A full-bridge inverter composed of four MOSFETs of TPH3208PS is used to generate square wave voltage. The square wave frequency is identical to the resonance frequency at 85 kHz. The radius of the road and receiver coils are 65 mm and 90 mm, respectively. They are all spiral coils and wounded from 400 strands of Litz wire. The ferrite is not used as the prototype is built to prove the feasibility of the proposed detuning method. The experimental parameters under inductive and capacitive detuning are listed in Table II.

The mutual inductance M_{ar1} and M_{pr} variation against the offset distance are shown in Fig. 16. As the receiver coil moves towards the repeater coil, M_{ar1} decreases gradually while M_{pr} increases. In AR charging mode, M_{ar1} is 13.8 μH and M_{pr} is 0.78 μH, while in PR charging mode, M_{ar1} is 0.12 μH and M_{pr} is 14.8 μH. As a result, it is reasonable to neglect M_{pr} in AR charging mode and M_{ar1} in PR charging mode.

C. Experimental Results of Different Detuning Types

The experiment results of the three charging modes shown in Fig. 17 are obtained from inductive and capacitive detuning systems. In Fig. 17(a), I_{rp} is the minimum compared to another two charging modes under inductive detuning condition. It is because the detuning impedance of the repeater coil is the largest in AR charging mode. Besides, the phase of I_{ac1} and I_{rp} is almost the same which is in agreement with (18) for Z_{rp} is a pure inductance reactance when the offset distance is zero. In Fig. 17(b), I_{rp} increases nearly by half due to the decrease in the inductance reactance of Z_{rp}, which can be explained as that part of the detuning impedance has been eliminated by the reflected impedance of the receiver. Meanwhile, I_{ac1} and I_{rp} have a slight phase difference for Z_{rp} contains both inductive reactance and resistance in APR charging mode based on (18). In Fig 17(c), the phase between I_{ac1} and I_{rp} continues to enlarge as the phase angle of Z_{rp} is minimized. In detail, the detuning impedance of the repeater coil is minimized while the real part of Z_{rp} is maximized in PR charging mode. It also can be known from Fig. 17(a)–(c) that the value of I_{re} is almost the same in the three charging modes, which shows that the output power in the three charging modes under the inductive detuning condition meets the requirement of quasi-constant output power. The experiment results of the three charging modes under capacitive detuning condition are shown in Fig. 17(d)–(f). In Fig. 17(d), the phase between I_{rp} and I_{ac1} is π according to (19) and the phase of I_{re} is entirely dependent on I_{ac1} for the power is mainly transferred by the channel of active coil in AR charging mode. In Fig. 17(e), I_{re} is almost 0 because the induced voltage generated by the active coil and repeater coil cancel each other out. The repeater coil is fully resonant in PR charging mode and the phase of I_{rp} has a 90° leading to I_{ac1} based on (18), as shown in Fig. 17(f). Compared to Fig. 17(e), the phase of I_{re} is 90° leading to that in Fig. 14(f) for the phase of I_{re} is entirely dependent on I_{rp} in PR charging mode. Based on the waveforms of I_{re} in Fig. 17(d)–(f),

TABLE IV
COMPARISONS OF DIFFERENT METHODS FOR THE DWPT SYSTEM PERFORMANCE

Reference	Number of Activated Coil	Number of Inverter	Primary Compensation Network	Minimum Efficiency	Continues Power transfer	Maximum Power Fluctuation	Additional Sensors
[16]	N	N	N*LCL	< 20%	No	/	Yes
[17]	N	N	3N*C+2N*L	< 60%	No	/	No
[26]	N	N/2	N*LCC	85%	Yes	50%	No
[27]	N	N	N*LCC	88%	/	10%	No
Proposed system	**N/2**	**N/2**	**N/2*LCL+N/2*LC**	**79%**	**Yes**	**8.5%**	**No**

"/" means not considered in the reference paper.

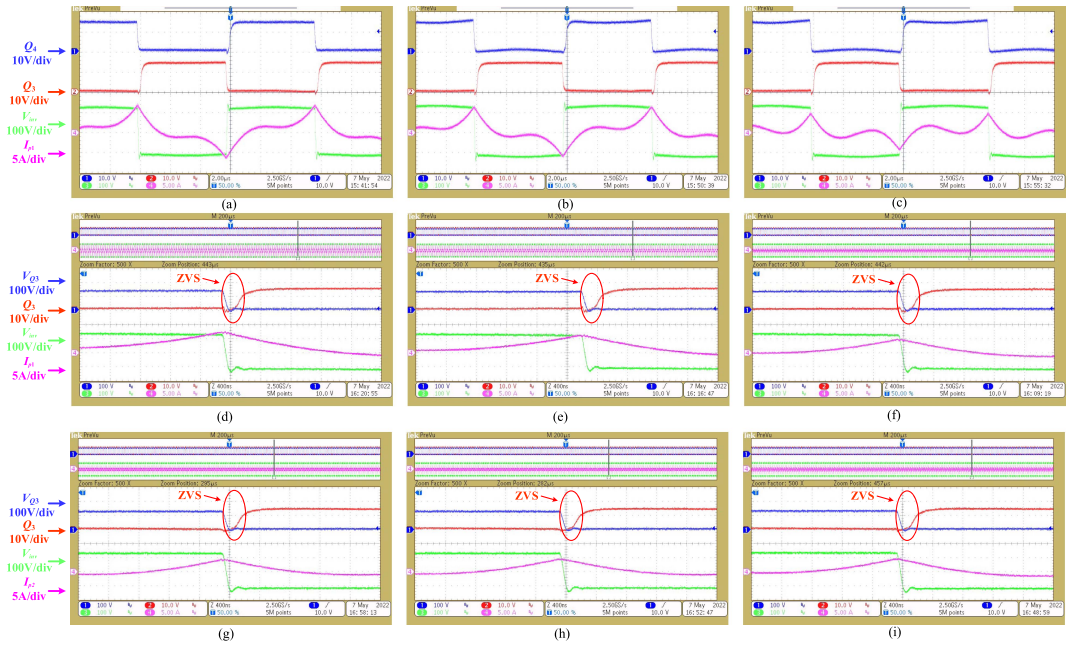

Fig. 22. Waveforms of drive signal Q_3, Q_4, V_{in}, I_{p1}, I_{p2}, and V_{Q3} in different charging modes: (a)–(c) Q_3, Q_4, $V_{\rm in}$, I_{p1} waveforms in all charging modes (inverter 1); (d)–(f) ZVS waveforms of Q_3 in all charging modes (inverter 1); (g)–(i) ZVS waveforms of Q_3 in all charging modes (inverter 2).

the switching of power transfer channel from the active coil to the repeater coil leads to drastic fluctuation in the output power under the case of capacitive detuning.

Fig. 18 shows the experimental results of an inductive detuning system during the whole dynamic process. In Fig. 18, I_{re} almost maintains constant from the beginning to the end, which indicates that the system can realize a smooth output power during the whole moving process. The waveforms of I_{ac1} and I_{rp} are symmetrical. It means the receiver moves from the active coil 1 to the repeater are symmetrical to the process that the receiver moves from the repeater to the next active coil.

Fig. 19 shows the simulation and experimental results of the output power and the system efficiency variation against the offset distances. The output power maintains 100 W with a maximum fluctuation of 8.5% and the maximum system efficiency is 85% in AR charging mode while the minimum system efficiency is 79% in PR charging mode. Under the condition of capacitive detuning, $P_{\rm out}$ decreases at first and is less than 1 W at the position of 60 mm and then, increases gradually. It is difficult to transfer power in APR charging mode. The theoretical and simulation results are in good agreement, which verifies the theoretical modeling and analysis.

D. Experiment Results of Different Detuning Rates

Inductive detuning is selected in this article and the value of the detuning rate α is selected as 0.31 following the design procedures in Fig. 13. $P_{\rm out}$ and the rms value of the repeater current under different detuning rates are shown in Fig. 20.

When $\alpha = 0.27$, $P_{\rm out}$ is higher than $P^*_{\rm out}$ and when $\alpha = 0.34$, $P_{\rm out}$ is lower than $P^*_{\rm out}$. Overall, the fluctuation of $P_{\rm out}$ is the minimum when α is 0.31. The lower α will raise $P_{\rm out}$ higher in APR and PR charging modes resulting in a higher repeater coil current from (6). In Fig. 20(b), the relationship of the repeater current under various α is $I_{rp\_\alpha\,=\,0.27} > I_{rp\_\alpha\,=\,0.31} > I_{rp\_\alpha\,=\,0.34}$. According to (12), the larger α can lead to a larger inductive reactance of Z_{rp}. Besides, I_{rp} increases at first and then decreases as the receiver coil moves towards the repeater coil. It can be known from (19), the variation tendency of I_{rp} is opposite to

that of Z_{rp}. This is in good agreement with the amplitude change curve of Z_{rp}, as shown in Fig. 6.

E. Experiment Results of Load Variation

Fig. 21 shows the output power $P_{\rm out}$ variation against the load R. According to Fig. 21, when the load variation is from -20% to $+20\%$, the power fluctuation is within $\pm 17.5\%$. A larger R will result in a higher $P_{\rm out,AR}$ and a lower $P_{\rm out,PR}$, and vice versa. The variation tendency of them is consistent with that in Fig. 12. The detailed data of this experiment can be found in Table III.

F. Experiment Results of ZVS

The proposed system is set inductive detuning not only for reducing power fluctuation but also for the realization of ZVS. β is set a little smaller than the value calculated by (13) to partly counteract the inductive impedance of the repeater coil. Thus, the proposed system contains inductive reactive power during the whole dynamic process. The realization of ZVS of the switches in all the charging modes is shown in Fig. 22. The waveforms from the top to the bottom are the drive signal of Q_3, Q_4, $V_{\rm in}$, I_{p1}, respectively. V_{Q3} is the voltage of drain to source (V_{DS}) of Q_3. In Fig. 22, when the switching Q_3 is turning OFF, Q_4 has not turned ON yet, I_{p1} is negative, which ensures the implementation of ZVS. The same situation occurs in both the inverters during all the charging modes. It is worth noting that states of the four switches of the phase-shift full-bridge are symmetrical. Thus, we choose Q_3 as an example. According to Fig. 22(d)–(f), Q_3 can realize ZVS in AR, APR, and PR charging modes. Thus, the four switches of inverter 1 can realize ZVS during the whole dynamic process. The situation is the same as inverter 2 according to Fig. 22(g)–(i).

G. Discussion and Comparison

Table IV shows the comparison results of the existing DWPT systems. Compare to the systems in Refs. [16], [17], [26], [27]. The proposed system uses the minimum number of inverter and resonant elements due to the introduction of passive repeater coils. A minimum power fluctuation can be realized in this paper through the method of detuning. Therefore, the proposed system can take low construction cost and good system performance into consideration at the same time. Thus, it is a promising choice in the dynamic wireless charging of AGVs.

V. Conclusion

This article proposed a detuning-repeater-based DWPT system that can achieve a quasi-constant output power during the dynamic process with reduced inverter count and lower construction costs. In the proposed system, half of the converter-driven active coils are replaced by simple passive repeater coils. The active and repeater coil alternately take the role of the main power transfer channel. A detuning method that introduces an imaginary impedance in both repeater and receiver circuits is adopted to help achieve quasi-constant output power. The currents of idle repeaters are suppressed by the detuning effect, reducing the no-load loss and benefiting the system safety. The repeater is automatically activated for power transfer when the it is eliminated by the reflected impedance of the receiver. The method of finding the boundary of the detuning rates under different system parameters is also given to optimize the selection of α and β. Following the proposed optimization design method based on the detuning rate, a 100 W experimental prototype has been established to verify the feasibility of the proposed DWPT system. The experimental results demonstrated that the proposed system can achieve a quasi-constant output power of 100 W with a maximum fluctuation of 8.5% and a system efficiency of around 82% during the entire dynamic process.

References

[1] Z. Zhang, H. Pang, A. Georgiadis, and C. Cecati, "Wireless power transfer—An overview," *IEEE Trans. Ind. Electron.*, vol. 66, no. 2, pp. 1044–1058, Feb. 2019.

[2] Z. Luo, S. Nie, M. Pathmanathan, and P. W. Lehn, "Exciter–Quadrature–Repeater transmitter for wireless electric vehicle charging with high lateral misalignment tolerance and low EMF emission," *IEEE Trans. Ind. Electron.*, vol. 7, no. 4, pp. 2156–2167, Dec. 2021.

[3] E. S. Lee, B. H. Choi, Y. H. Sohn, G. C. Lim, and C. T. Rim, "Multiple dipole receiving coils for 2-D omnidirectional wireless mobile charging under wireless power zone," in *Proc. IEEE Energy Convers. Congr. Expo.*, Sep. 2015, pp. 3209–3214.

[4] M. R. Basar, M. Y. Ahmad, J. Cho, and F. Ibrahim, "An improved wearable resonant wireless power transfer system for biomedical capsule endoscope," *IEEE Trans. Ind. Electron.*, vol. 65, no. 10, pp. 7772–7781, Oct. 2018.

[5] A. Ahmad, M. S. Alam, and R. Chabaan, "A comprehensive review of wireless charging technologies for electric vehicles," *IEEE Trans. Transp. Electrif.*, vol. 4, no. 1, pp. 38–63, Mar. 2018.

[6] S. Huang, T. Lee, W. Li, and R. Chen, "Modular on-road AGV wireless charging systems via interoperable power adjustment," *IEEE Trans. Ind. Electron.*, vol. 66, no. 8, pp. 5918–5928, Aug. 2019.

[7] Z. Liu, M. Su, Q. Zhu, L. Zhao, and A. P. Hu, "A dual frequency tuning method for improved coupling tolerance of wireless power transfer system," *IEEE Trans. Power Electron.*, vol. 36, no. 7, pp. 7360–7365, Jul. 2021.

[8] F. J. López-Alcolea, J. V. d. Real, P. Roncero-Sánchez, and A. P. Torres, "Modeling of a magnetic coupler based on Single- and Double-Layered rectangular planar coils with in-plane misalignment for wireless power transfer," *IEEE Trans. Power Electron.*, vol. 35, no. 5, pp. 5102–5121, May 2020.

[9] L. Zhao, D. J. Thrimawithana, U. K. Madawala, A. P. Hu, and C. C. Mi, "A misalignment-tolerant series-hybrid wireless EV charging system with integrated magnetics," *IEEE Trans. Power Electron.*, vol. 34, no. 2, pp. 1276–1285, Feb. 2019.

[10] D. Patil, M. K. McDonough, J. M. Miller, B. Fahimi, and P. T. Balsara, "Wireless power transfer for vehicular applications: Overview and challenges," *IEEE Trans. Transp. Electrif.*, vol. 4, no. 1, pp. 3–37, Mar. 2018.

[11] A. C. Bagchi, A. Kamineni, R. A. Zane, and R. Carlson, "Review and comparative analysis of topologies and control methods in dynamic wireless charging of electric vehicles," *IEEE J. Emerg. Sel. Topics Power Electron.*, vol. 9, no. 4, pp. 4947–4962, Aug. 2021.

[12] G. Buja, M. Bertoluzzo, and H. K. Dashora, "Lumped track layout design for dynamic wireless charging of electric vehicles," *IEEE Trans. Ind. Electron.*, vol. 63, no. 10, pp. 6631–6640, Oct. 2016.

[13] K. Kim, J. Kim, H. Kim, J. Ahn, H. H. Park, and S. Ahn, "Evaluation of electromagnetic field radiation from wireless power transfer electric vehicle," in *Proc. Int. Symp. Antennas Propag.*, 2016, pp. 40–41.

[14] Z. Zhang, H. Pang, A. Georgiadis, and C. Cecati, "Wireless power transfer—An overview," *IEEE Trans. Ind. Electron.*, vol. 66, no. 2, pp. 1044–1058, Feb. 2019.

[15] K. B. Lee, Z. Pantic, and S. M. Lukic, "Reflexive field containment in dynamic inductive power transfer systems," *IEEE Trans. Power Electron.*, vol. 29, no. 9, pp. 4592–4602, Sep. 2014.

[16] X. Dai, J. Jiang, and J. Wu, "Charging area determining and power enhancement method for multiexcitation unit configuration of wirelessly dynamic charging EV system," *IEEE Trans. Ind. Electron.*, vol. 66, no. 5, pp. 4086–4096, May 2019.

[17] S. Y. Jeong, J. H. Park, G. P. Hong, and C. T. Rim, "Autotuning control system by variation of self-inductance for dynamic wireless EV charging with small air gap," *IEEE Trans. Power Electron.*, vol. 34, no. 6, pp. 5165–5174,

[18] P. K. S. Jayathurathnage, A. Alphones, D. M. Vilathgamuwa, and A. Ong, "Optimum transmitter current distribution for dynamic wireless power transfer with segmented array," *IEEE Trans. Microw. Theory Tech.*, vol. 66, no. 1, pp. 346–356, Jan. 2018.
[19] M. Budhia, J. T. Boys, G. A. Covic, and C. Huang, "Development of a single-sided flux magnetic coupler for electric vehicle IPT charging systems," *IEEE Trans. Ind. Electron.*, vol. 60, no. 1, pp. 318–328, Jan. 2013.
[20] L. Zhao, D. J. Thrimawithana, and U. K. Madawala, "Hybrid bidirectional wireless EV charging system tolerant to pad misalignment," *IEEE Trans. Ind. Electron.*, vol. 64, no. 9, pp. 7079–7086, Sep. 2017.
[21] Y. Liu, R. Mai, D. Liu, Y. Li, and Z. He, "Efficiency optimization for wireless dynamic charging system with overlapped DD coil arrays," *IEEE Trans. Power Electron.*, vol. 33, no. 4, pp. 2832–2846, Apr. 2018.
[22] L. Chen, G. R. Nagendra, J. T. Boys, and G. A. Covic, "Double-Coupled systems for IPT roadway applications," *IEEE J. Emerg. Sel. Topics Power Electron.*, vol. 3, no. 1, pp. 37–49, Mar. 2015.
[23] S. Choi, J. Huh, W. Y. Lee, S. W. Lee, and C. T. Rim, "New cross-segmented power supply rails for roadway-powered electric vehicles," *IEEE Trans. Power Electron.*, vol. 28, no. 12, pp. 5832–5841, Dec. 2013.
[24] Y. Yao, Y. Wang, X. Liu, F. Lin, and D. Xu, "A novel parameter tuning method for a double-sided LCL compensated WPT system with better comprehensive performance," *IEEE Trans. Power Electron.*, vol. 33, no. 10, pp. 8525–8536, Oct. 2018.
[25] H. Feng, T. Cai, S. Duan, X. Zhang, H. Hu, and J. Niu, "A dual-side-detuned series–series compensated resonant converter for wide charging region in a wireless power transfer system," *IEEE Trans. Ind. Electron.*, vol. 65, no. 3, pp. 2177–2188, Mar. 2018.
[26] Q. Zhu, L. Wang, Y. Guo, C. Liao, and F. Li, "Applying LCC compensation network to dynamic wireless EV charging system," *IEEE Trans. Ind. Electron.*, vol. 63, no. 10, pp. 6557–6567, Oct. 2016.
[27] H. Feng, T. Cai, S. Duan, J. Zhao, X. Zhang, and C. Chen, "An LCC-Compensated resonant converter optimized for robust reaction to large coupling variation in dynamic wireless power transfer," *IEEE Trans. Ind. Electron.*, vol. 63, no. 10, pp. 6591–6601, Oct. 2016.

Wenjing Xiong (Member, IEEE) was born in Hunan, China, in 1991. She received the B.S. degree in automation and the Ph.D. degree in control science and engineering from Central South University, Changsha, China, in 2012 and 2017, respectively.

She is currently an Associate Professor with the School of Automation, Central South University, China. Her research interests include modulation strategy for power converters, matrix converter, ac/dc converter, and wireless power transfer.

Qihui Yu was born in Jiangxi, China, in 1998. He received the B.S. degree in electrical engineering and automation in 2020 from Central South University, Changsha, China, where he is currently working toward the M.S. degree in electrical engineering and automation with the Department of Automation.

His research interest includes wireless power transfer.

Mr. Yu was the recipient of the Top 10 1st Stage Proposal Award in Inaugural IEEE Global Student Wireless Power Competition, in 2022.

Zixi Liu received the B.S. degree in electrical engineering and automation from Sichuan University, Chengdu, China, in 2016, and the M.S. degree in software engineering in 2019 from Central South University, Changsha, China, where he is currently working toward the Ph.D. degree in control science and engineering with Department of Automation.

His research interest includes wireless power transfer.

Mr. Liu was the recipient of the Top 10 1st Stage Proposal Award in the Inaugural IEEE Global Student Wireless Power Competition, in 2022.

Lei Zhao (Member, IEEE) received the B.S. degree from the Xi'an University of Technology, Xi'an, China, in 2011, the M.E. degree from The University of Auckland, Auckland, New Zealand, in 2013, both in electrical engineering, and the Ph.D. degree in electrical and electronic engineering from The University of Auckland in 2019.

He was a Research Fellow with the Department of Electrical, Computer, and Software Engineering, The University of Auckland, from 2019 to 2021, was with Prof. A. P. Hu. In 2022, he was with the Automation School, Chongqing University, Chongqing, China, where he is currently working as an Associate Professor. His research interests include bidirectional hybrid inductive power transfer systems for electrical vehicle charging and high frequency power electronics.

Qi Zhu received the B.S. degree in electrical engineering and automation and the Ph.D. degree in control science and engineering from Central South University, Changsha, China, in 2014 and 2019, respectively.

He was a Joint Ph.D. Student from 2017 to 2019, and a Research Fellow from 2019 to 2021, both under the supervision of Prof. A. P. Hu with the University of Auckland, Auckland, New Zealand. From 2022, he is currently a Senior Hardware R&D Engineer with Xiaomi, Beijing, China.

His research interests include wireless power transfer, power electronics, and renewable energy.

Mei Su (Member, IEEE) was born in Hunan, China, in 1967. She received the B.S., M.S., and Ph.D. degrees from the School of Information Science and Engineering, Central South University, Changsha, China, in 1989, 1992, and 2005, respectively.

She is currently a Full Professor with the School of Automation, Central South University. She is currently an Associate Editor for the IEEE TRANSACTIONS ON POWER ELECTRONICS. Her research interests include matrix converter, adjustable speed drives, and wind energy conversion system.